

RuPd Alloy Nanoparticles Supported on N-Doped Carbon as an Efficient and Stable Catalyst for Benzoic Acid Hydrogenation

Minghui Tang, Shanjun Mao, Mingming Li, Zhongzhe Wei, Fan Xu, Haoran Li, and Yong Wang

ACS Catal., Just Accepted Manuscript • DOI: 10.1021/acscatal.5b00037 • Publication Date (Web): 14 Apr 2015

Downloaded from <http://pubs.acs.org> on April 19, 2015

Just Accepted

“Just Accepted” manuscripts have been peer-reviewed and accepted for publication. They are posted online prior to technical editing, formatting for publication and author proofing. The American Chemical Society provides “Just Accepted” as a free service to the research community to expedite the dissemination of scientific material as soon as possible after acceptance. “Just Accepted” manuscripts appear in full in PDF format accompanied by an HTML abstract. “Just Accepted” manuscripts have been fully peer reviewed, but should not be considered the official version of record. They are accessible to all readers and citable by the Digital Object Identifier (DOI®). “Just Accepted” is an optional service offered to authors. Therefore, the “Just Accepted” Web site may not include all articles that will be published in the journal. After a manuscript is technically edited and formatted, it will be removed from the “Just Accepted” Web site and published as an ASAP article. Note that technical editing may introduce minor changes to the manuscript text and/or graphics which could affect content, and all legal disclaimers and ethical guidelines that apply to the journal pertain. ACS cannot be held responsible for errors or consequences arising from the use of information contained in these “Just Accepted” manuscripts.



RuPd Alloy Nanoparticles Supported on N-Doped Carbon as an Efficient and Stable Catalyst for Benzoic Acid Hydrogenation

*Minghui Tang, Shanjun Mao, Mingming Li, Zhongzhe Wei, Fan Xu, Haoran Li and Yong Wang**

Advanced Materials and Catalysis Group, ZJU-NHU United R&D Center, Department of Chemistry, Zhejiang University, Hangzhou 310028, P. R. China

KEYWORDS: Bimetallic catalyst, RuPd alloy, N-doped carbon, Chemoselective hydrogenation, Benzoic acid

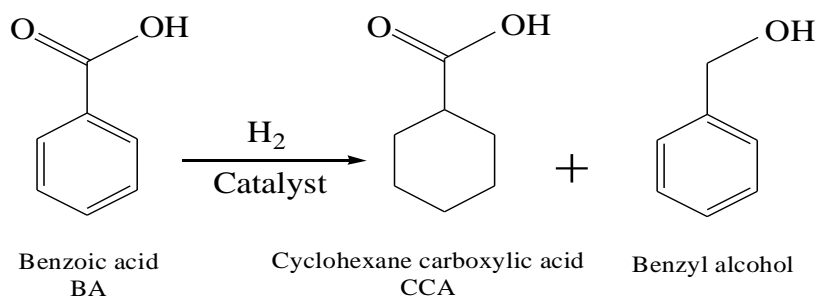
ABSTRACT: RuPd alloy nanoparticles (3.6 nm) uniformly dispersed on N-doped carbon (RuPd/CN) was prepared via a simple ultrasound-assisted co-reduction method. The RuPd/CN is highly active, selective and stable in the hydrogenation of benzoic acid to cyclohexane carboxylic acid under mild conditions with a TOF up to 2066 h⁻¹. It was found that the bimetallic RuPd/CN catalyst exhibited a substantially enhanced activity compared with the monometallic catalysts (Ru/CN and Pd/CN). The reason for higher performance of the RuPd/CN catalyst is considered to be the increased Ru⁰/Ruⁿ⁺ ratio induced by the electronic interaction between Ru and Pd as evidenced by various characterizations. Notably, the different phenomenon of activity platform on different catalysts ascribed to the effect of hydrogen pressure was newly observed and further explained by the first-principle studies. Moreover, the factors influencing the

adsorption modes of BA, especially the configuration of the carboxyl group are investigated preliminarily in first-principle giving a distinct insight from the former work. The reason why the carboxyl group in benzoic acid does not undergo hydrogenation, which results in the superior selectivity (>99%), is also revealed by the comparison of the thermodynamics of hydrogenation and dissociation of the carboxyl group.

1. INTRODUCTION

Cyclohexane carboxylic acid (CCA) is an important organic intermediate for the synthesis of pharmaceuticals, such as praziquantel, hexanolactam and ansatrienin.¹ Chemoselective hydrogenation of benzoic acid (BA) is the most effective method to obtain CCA (Scheme 1).² However, aromatic ring hydrogenation requires more severe conditions than those required to hydrogenate other functional groups (typically, C=O, C=C, or C=N etc.) due to the need to overcome the high resonance energy of benzene ring.³

Scheme 1. Products from divergent pathways of hydrogenation of BA.



Traditionally, hydrogenation of BA has been carried out by using stoichiometric Na-K alloys.⁴ It also has been found that CCA can be produced from hydrogenation of molten BA without any solvent over carbon-supported precious metals catalyst. Unfortunately, the reaction was usually

1
2
3 carried out in scCO₂ or under high H₂ pressures (10~15 MPa) and high temperatures (150~200
4 °C).⁵ Thus, preparing a high-performance and environmentally friendly catalyst used under mild
5
6
7
8 reaction conditions for the chemoselective hydrogenation of BA is urgently needed.
9

10 In recent years, researchers have found that Pd can be used for selective hydrogenation
11 reactions. Activity of Pd catalysts can be controlled by varying the support materials (MgO,⁶
12 Al₂O₃,⁷ activated carbon,⁸ TiO₂,⁹ MCM-41,¹⁰ mpg-C₃N₄ etc.¹¹⁻¹⁴). As carbon materials are
13
14
15
16
17
18
19
20
21
22
23
24
25
26
27
28
29
30
31
32
33
34
35
36
37
38
39
40
41
42
43
44
45
46
47
48
49
50
51
52
53
54
55
56
57
58
59
60
“sustainable” support materials for Pd nanoparticles (NPs).¹⁵ However, as reported by Anderson,
the carbon supported Pd catalyst also presented a poor activity toward the aromatic ring
hydrogenation, the activated carbon supported Pd (Pd/AC) converted only 34% BA to CCA after
24 h using 1 bar hydrogen at 85 °C.¹⁶ Furthermore, Pd deposited on carbons easily leaches during
catalytic processes because the interaction between the metal and the carbon surface is weak. As
a consequence, the chemical or catalytic properties of carbons do not always satisfy the sharply
increasing demands of catalysis. The recent fast-growing research upon porous carbon materials,
especially the nitrogen doped carbon, with enhanced chemical, electrical and functional
properties, demonstrated as a novel support for heterogeneous catalysis.¹⁷⁻²⁴

Indeed, we showed earlier that Pd NPs supported on a N-doped carbon (Pd/CN) catalysed BA
hydrogenation efficiently, obtaining 100% yield of CCA at 85 °C under 1 bar H₂ pressure after
24 hours.²⁵ However, the high price of noble metal catalysts has limited their further application
in industry. Therefore, it is desired to search out a suitable substitute for Pd having lower cost but
comparable activity for the BA hydrogenation. Alloying with a second metal is considered to be
effective for obtaining a highly active catalyst.²⁶⁻²⁸ In addition, the dilution of costly noble metals

1
2
3 by inexpensive metals in bimetallic catalysts is also of interest because of the potential savings in
4 material cost, while still maintaining or even enhancing the catalytic performance.²⁹⁻³³
5
6

7
8 Herein, considering of the bimetallic effects and the advantage of lowering the cost of catalyst,
9 we prepared bimetallic RuPd/CN catalyst, and tested its activity in the hydrogenation of BA. We
10 found that bimetallic catalyst RuPd/CN exhibited higher activity than monometallic catalysts
11 Ru/CN and Pd/CN. An obvious electronic interaction between Ru and Pd was observed through
12 XPS, verifying the reason for better catalytic behavior of bimetallic catalyst in the hydrogenation
13 reaction. The intrinsic alloy synergistic effects on the catalyst structure and catalysis behavior
14 were investigated in deep both experimentally and theoretically. Furthermore, the as-synthesized
15 RuPd/CN not only exhibits higher activity, but also better stability towards BA hydrogenation,
16 when compared with Pd/CN, Ru/CN and commercial Pd/AC catalysts.
17
18
19
20
21
22
23
24
25
26
27
28
29
30
31

32 **2. RESULTS AND DISCUSSION**

33
34 We have reported that Pd/CN showed higher catalytic performance in BA hydrogenation to
35 CCA than other supported Pd catalysts (Pd/AC, Pd/metal oxide, etc).²⁵ The performance of
36 various Pd/CN catalysts modified with inexpensive metals (Ru, Cu, Fe, Ni and In) was compared
37 as shown in Table 1. In the bimetallic catalysts, the loading of Pd was fixed at 1 wt. %; the
38 amount of additive metal was fixed at 2.5 by the weight ratio of the additive to Pd, which is the
39 best composition for RuPd/CN (Table S1). Notably, RuPd/CN showed the highest BA
40 conversion, even compared with Pd/CN. Unfortunately, other MPd/CN (M=Cu, Fe, Ni, and In)
41 all showed very poor activity. Furthermore, the performance of various metals (Ru, Cu, Fe, Ni
42 and In) modified Ru/CN catalysts was also compared. As might be expected, RuPd/CN showed
43 the highest BA conversion, but other RuM/CN (M= In, Fe, Cu, and Ni) showed relatively poor
44
45
46
47
48
49
50
51
52
53
54
55
56
57
58
59
60

activity. From a catalytic point of view, the RuPd/CN catalyst already appears as quite a unique and interesting material. Next, a series of characterizations and activity tests accompanied by theoretical calculations had been carried out to explain the experimental results and find out the relationship between bimetallic catalyst intrinsic alloy synergistic effect and catalytic properties.

Table 1. Comparison of the catalytic performances in the BA hydrogenation over modified Pd/CN (1 wt. % Pd, secondary metal/Pd=2.5) and modified Ru/CN (1 wt. % M, M/Pd=2.5). ^a

Entry	Catalyst	Conversion/% and (selectivity %)
1	Pd/CN	38(100)
2	CuPd/CN	0
3	FePd/CN	0
4	NiPd/CN	0
5	InPd/CN	0
6	RuPd/CN	67(100)
7	Ru/CN	9(100)
8	RuIn/CN	0.2(100)
9	RuFe/CN	10(100)
10	RuNi/CN	11(100)
11	RuCu/CN	4(100)

^a Reaction conditions: BA 0.5 mmol, catalyst 50 mg, solvent water 25 mL, 85 °C, 0.1MPa H₂, 6 hours.

In order to highlight the advantage of N-doped carbon as support, a variety of non-nitrogen carbon (non-nitrogen hydrothermal carbon, HC; commercial active carbon, AC; commercial multi-wall carbon nanotubes, CNT) are used to compare with CN under identical conditions

(Table 2). The textural properties of the different catalysts are listed in [Table S2](#). Among the different catalysts, RuPd/CN was found to give the most active system (Table 2, entry 1). To clarify, the HC (from glucose) was prepared using the same method as CN (D-glucosamine hydrochloride). RuPd/HC resulted in a BA conversion of only 28%, meaning the N atoms in RuPd/CN are of crucial importance on the catalytic activity. Thus, N-doped carbon materials as high-performance catalyst supports have great promising application in heterogeneous catalysis.

Table 2. Catalytic results for different catalysts. ^a

Entry	Catalyst	Conversion/% and (selectivity / %)
1	RuPd/CN	67(100)
2	RuPd/HC	28(100)
3	RuPd/AC	45(100)
4	RuPd/CNT	39(100)

^a Reaction conditions: BA 0.5 mmol, catalyst 50 mg, solvent water 25 mL, 85 °C, 0.1MPa H₂, 6 hours.

The mesoporous structure of the support and various catalysts were identified by nitrogen adsorption/desorption isotherms ([Figure S4](#), [Table S2](#)). The results clearly show the support CN retained its mesoporosity well after the loading of monometallic or bimetallic nanoparticles, indicating that the CN was an excellent support.

To better understand the catalytic properties of supported bimetallic catalysts, it is necessary to explore both the distribution and the chemical states of the metals within the individual NPs. The dispersion and the average metal particle size of the RuPd/CN were confirmed by HRTEM

1
2
3 (Figure 1). It revealed that the NPs were uniformly dispersed on the support, no significant
4 aggregations were observed, which may result from the excellent anchoring of the CN towards
5 the deposited NPs due to the electronegative nitrogen in the carbon structure.¹⁵ For the Pd/CN,
6 the metal particles had an average size of 4.6 nm with a range of 2~8 nm (Figure S5), while
7 RuPd/CN exhibited a smaller particle size (3.6 nm) and a relatively narrow particle size
8 distribution (2~5 nm), indicating that the introduction of Ru could effectively improve the Pd
9 dispersion. Figure 1 (C) shows the particles were highly faceted. The nanocrystal plane spacing
10 was measured as 0.199 nm, which locates between the Ru (111) of 0.129 nm and the Pd (111) of
11 0.224 nm. Furthermore, no separated Ru or Pd lattice was detected, which demonstrated Ru and
12 Pd distributed homogenously in the particles of RuPd/CN.
13
14
15
16
17
18
19
20
21
22
23
24
25
26

27 In addition, STEM analysis was performed to clarify the structural and compositional details
28 of RuPd NPs (Figure 2). The color distribution in HAADF images showed that the Ru and Pd X-
29 ray signals completely homogeneous cover the spatial area of the NPs, suggesting that the alloy
30 has been formed. EDX line scanning analysis of two optionally neighbored RuPd NPs further
31 verified the formation of atomic-level RuPd alloy.
32
33
34
35
36
37
38
39
40
41
42
43
44
45
46
47
48
49
50
51
52
53
54
55
56
57
58
59
60

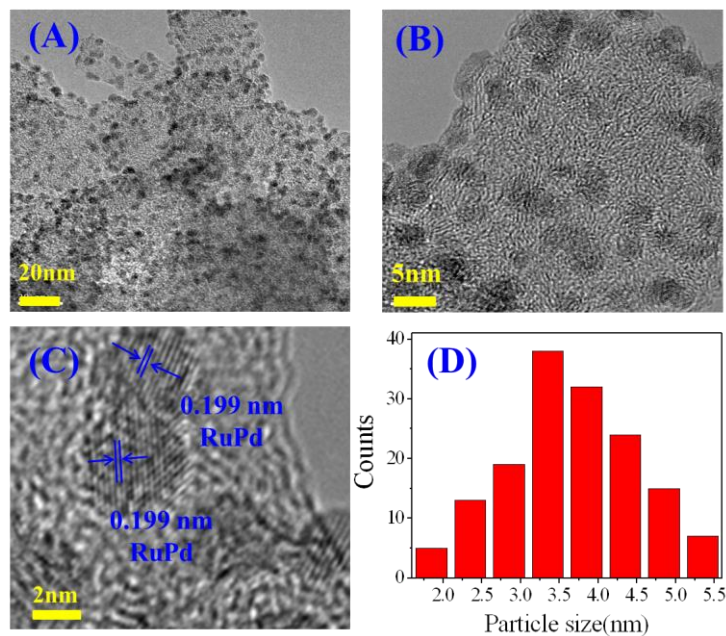


Figure 1. HRTEM images (A, B and C) and particle size distribution (D) of RuPd/CN.

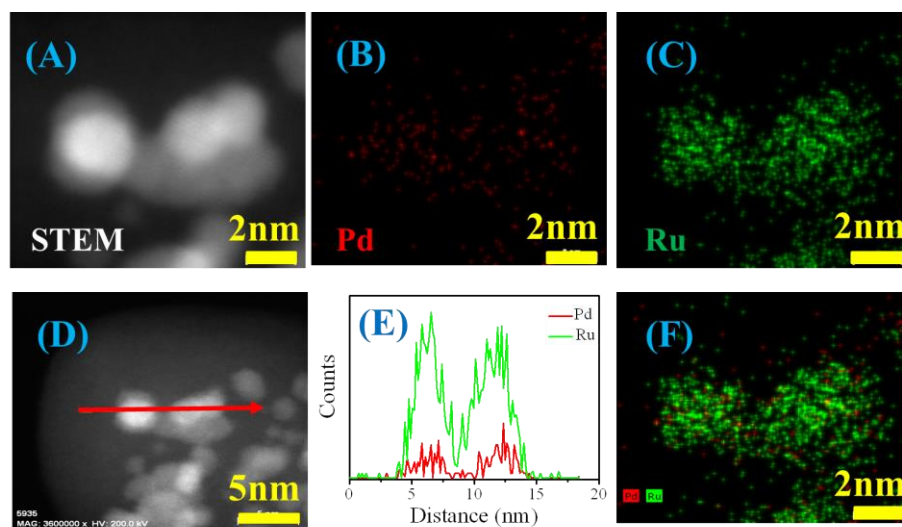
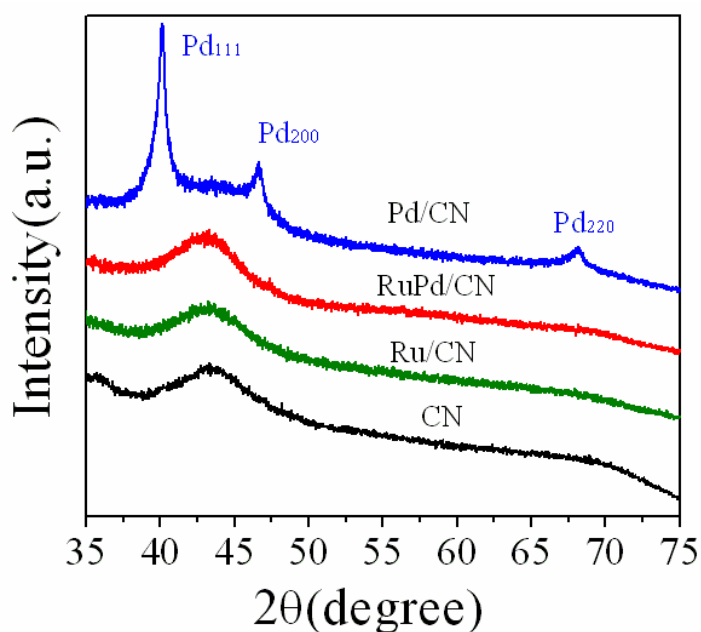


Figure 2. (A) HAADF-STEM image, (B) Pd-L and (C) Ru-L STEM-EDX map obtained from a group of RuPd NPs of RuPd/CN. (F) Reconstructed overlay images of the maps shown in panels (B) and (C), red, Pd; green, Ru. (E) Compositional line profiles of Pd and Ru for the RuPd NPs recorded along the arrow shown in the STEM image (D).

1
2
3 The XRD patterns of various samples are shown in Figure 3. All samples present a broadened
4 peak centered at 43.2°, which could be assigned to the CN support. Diffraction peaks of Pd/CN
5
6 peak centered at 43.2°, which could be assigned to the CN support. Diffraction peaks of Pd/CN
7
8 at 2θ of 40.1°, 46.7° and 68.1° are indexed to the (111), (200) and (220) crystal planes of Pd,
9
10 respectively. These peaks indicate that the deposited Pd of Pd/CN catalyst has a face-centered
11
12 cubic (fcc) structure.³⁴ However, no characteristic peaks of Ru can be fitted in the XRD patterns
13
14 of Ru/CN, indicating that the Ru NPs are less than 4 nm in size and well dispersed on the support,
15
16 which is also in agreement with the HRTEM results (Figure S6).³⁵ Moreover, no peaks
17
18 corresponding to Ru and Pd are detected in the RuPd/CN catalysts, which demonstrate that the
19
20 Ru and Pd form a RuPd alloy with very small particle size along with a good dispersion on the
21
22 support, which is also in accordance with the HRTEM results.



53
54
55
56
57
58
59
60

Figure 3. XRD patterns of different catalysts.

To get further insight into the interactions between Ru and Pd, XPS investigations were then conducted (Figure 4). The binding energies are corrected with reference to the C 1s line at 284.5

1
2
3 eV. As shown in Figure 4 (A), an obvious positive shift (0.2~0.5 eV) in binding energy can be
4 observed for RuPd/CN with respect to Pd/CN, indicating a change in the electronic properties of
5 Pd caused by the alloying effect between Ru and Pd, which can be also certified by the binding
6 energy shift of Ru. As the Ru 3d_{3/2} peak overlaps with that of C 1s on support CN, Ru 3p peak
7 are employed for all samples to determine the chemical state of Ru.^{36, 37, 38} Compared with
8 Ru/CN, the binding energy of Ru 3p_{3/2} for RuPd/CN presented a negative shift (0.2~0.3 eV) after
9 the formation of RuPd alloy.
10
11
12
13
14
15
16
17
18
19

20 For a more detailed understanding of the XPS measurements, Table 3 summarized the XPS-
21 derived ratios of oxidized and reduced metal states with different catalysts, giving evidence of
22 the surface Pd electronic state changes induced by the addition of Ru. It was found that, contrast
23 to monometallic catalysts (Pd/CN and Ru/CN), the ratio of Pd⁰/Pd²⁺ decreased while the ratio of
24 Ru⁰/Ruⁿ⁺ increased for the bimetallic catalyst (RuPd/CN), confirming that the existence of Pd
25 promoted the reduction of Ruⁿ⁺. In conclusion, such shifts suggest that electronic status of Ru
26 and Pd modulated as a result of alloy formation, thereby influencing the catalytic behavior of Pd
27 in the hydrogenation reaction. This will be further confirmed by the catalyst evaluation results
28 described below.
29
30
31
32
33
34
35
36
37
38
39

40 H₂-TPR experiments are performed to further confirm the interaction between Ru and Pd
41 (Figure 5). The Pd/CN presents a single large hydrogen release peak centered at 70 °C, which is
42 caused by the decomposition of palladium hydride (PdH_x), indicating the easy reducibility of
43 Pd²⁺.^{16, 31, 39} However, the reduction profile of the Ru/CN catalyst shows two hydrogen
44 consumption peaks with maximum at about 78 °C and 134 °C, demonstrating two types of
45 ruthenium oxides might have been formed on the Ru/CN catalyst.⁴⁰ For the bimetallic catalyst
46 RuPd/CN, only a weak and broad hydrogen consumption peak in the temperature ranges 60~117
47
48
49
50
51
52
53
54
55
56
57
58
59
60

°C was observed, revealing that interaction occurred between Ru and Pd. We deduce that this peak may be related to the reduction of Ru oxides. Thus, the existence of Pd metal helps the reduction of ruthenium oxides, in agreement with the XPS analysis.

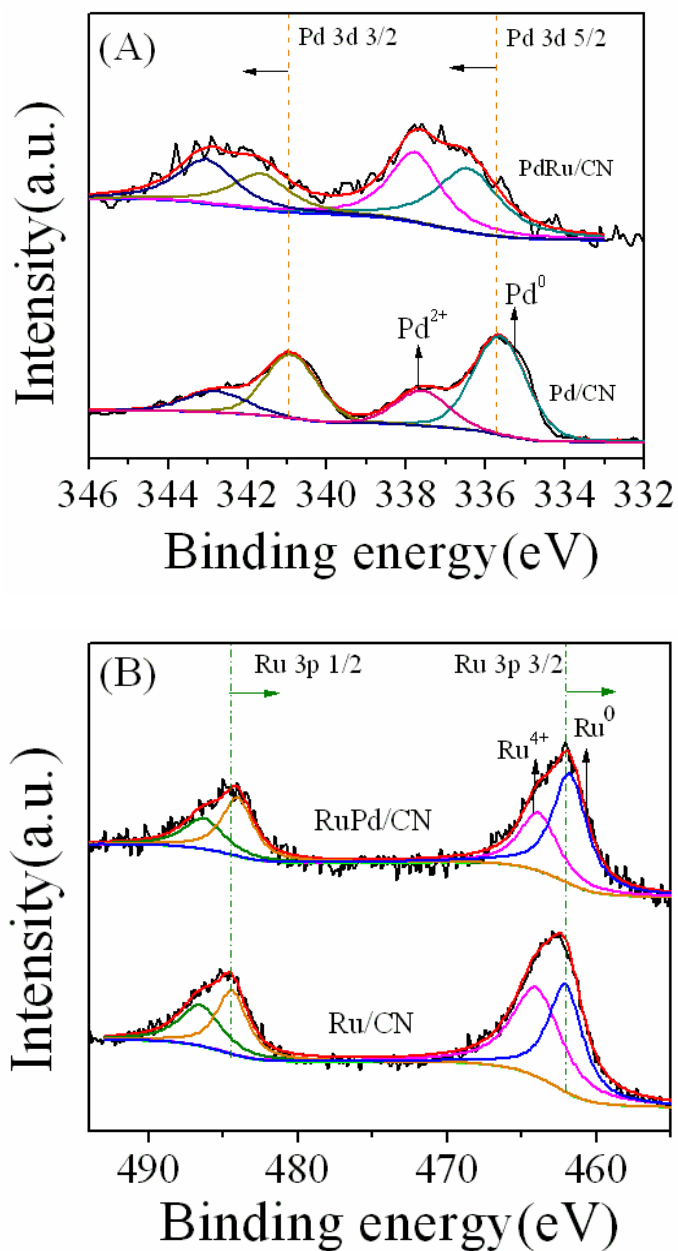
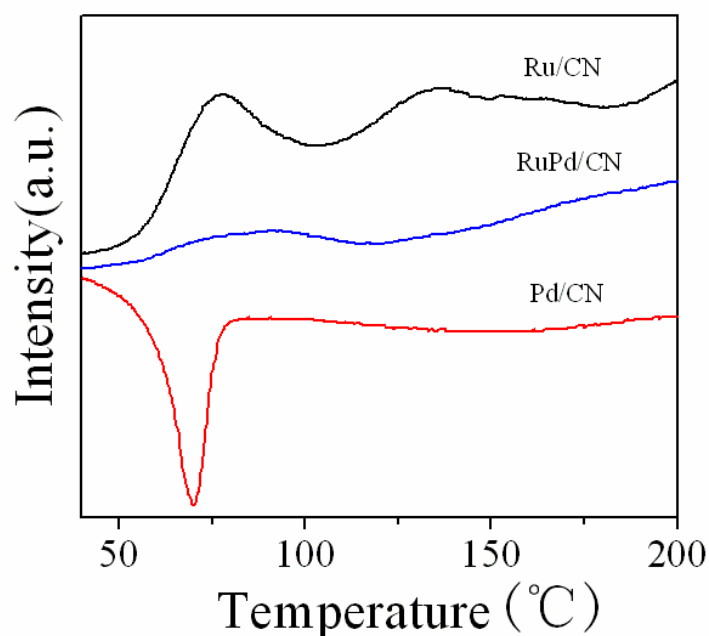


Figure 4. XPS spectra of Pd 3d (A) and Ru 3p (B) in the different catalysts.

Table 3. Binding energies (eV) and curve fitting results of Pd 3d and Ru 3p XPS spectra.

Catalyst	Pd 3d5/2(eV)		Ru 3p3/2(eV)		Relative percentage (%)	
	Pd ²⁺	Pd ⁰	Ru ⁿ⁺	Ru ⁰	Pd ⁰ /Pd ²⁺	Ru ⁰ /Ru ⁿ⁺
Pd/CN	337.6	335.6	-	-	72/28	-
RuPd/CN	337.8	336.1	463.8	461.8	52/49	62/38
Ru/CN	-	-	464.0	462.1	-	48/52

**Figure 5.** H₂-TPR patterns of CN supported Pd, Ru and RuPd catalysts.

Having proved the successfully preparation of RuPd/CN catalyst with Ru and Pd finely alloyed together with small size, then the catalytic performance are tested in the hydrogenation of BA to CCA. As shown in Table 4, under the given mild reaction conditions, both Ru/CN and Pd/CN showed low BA conversion, whereas RuPd/CN exhibited a relatively high conversion of 67%. Indeed, this phenomenon results from the remarkably promotion effect of RuPd alloy

1
2
3 formation. We also prepared Ru[^]Pd/CN through an ultrasound-assisted two step reduction
4 method (see [Supporting Information](#)), which also presented a lower catalytic performance
5 compared with the co-reduction method prepared RuPd/CN (Table 4, entry 5), suggesting the
6 synergistic effect of Ru and Pd generated during the process of preparation. In consequence, the
7 highly efficient catalytic performance of RuPd/CN inspired us to perform the scale-up
8 experiment (Table 4, entry 4). In this typical process, BA can almost completely selective
9 hydrogenation to CCA within 2 hours, achieving a relatively high turn-over frequencies (TOFs)
10 of 2066 h⁻¹.
11
12
13
14
15
16
17
18
19
20
21
22
23
24

25 **Table 4.** BA Hydrogenation with different catalyst. ^a

Entry	Catalyst	Conversion/% and (selectivity %)	TOF (h ⁻¹) _{Pd} ^b
1	Pd/CN	38(100)	1.7
2	Ru/CN	9(100)	-
3	RuPd/CN	67(100)	11.5
4 ^c	RuPd/CN	100(100)	2066
5 ^d	Ru [^] Pd/CN	52(100)	8.9

26
27
28
29
30
31
32
33
34
35
36
37
38
39
40
41
42
43
44 ^a Reaction conditions: BA 0.5 mmol, catalyst 50 mg, solvent water 25 mL, 85 °C, 0.1 MPa H₂, 6
45 hours. ^b Obtained by assuming that the Pd atoms were solely responsible for the activity. ^c
46 Reaction conditions: BA 10 mmol, catalyst 25 mg, solvent water 50 mL, 100 °C, 5 MPa H₂, 2
47 hours. ^d This catalyst was prepared by an ultrasound-assisted two step reduction method (see
48 Supporting Information).
49
50
51
52
53
54
55
56
57
58
59
60

1
2
3 The effects of hydrogen pressure on the activity of different catalysts were investigated as
4 shown in Figure 6 (A). Interestingly, the activity of RuPd/CN and Ru/CN both increased along
5 with the elevated pressure, while an activity platform of Ru/CN emerges at 0.8 MPa H₂ pressure.
6
7 Pd/CN shows the lowest activity to BA hydrogenation. The increase of H₂ pressure has rare
8 impact on the activity of Pd/CN, since the earliest platform appeared at 0.4 MPa. In order to
9 further understand the platform phenomenon newly found, the adsorption energies of BA on Pd,
10 Ru and RuPd alloy are calculated respectively, hoping to obtain a preliminary explanation (The
11 relevant adsorption modes are shown in [Figure S2](#)). As is shown in Figure 6 (B), BA displays no
12 affinity to the Pd surface with small positive adsorption energy. This indicates the low
13 concentration of the chemisorbed BA and explains the resulted early platform on Pd/CN catalyst
14 since the Pd surface is mostly covered by dissociated H atoms. However, the chemisorption of
15 BA on the other two catalysts is rather favorable, with the adsorption energies of -0.7 eV and -
16 1.29 eV for Ru and RuPd, respectively. The notable adsorption energies make a competitive
17 chemisorption between BA and H₂, thus the platform for Ru/CN catalyst appears later, and that
18 for RuPd/CN catalyst never shows the platform during the investigated H₂ pressure range due to
19 the relatively large adsorption energy. Electronic structure was then performed to enlighten the
20 origin of different adsorption energies. Results showed that the electron transfer between BA and
21 the catalysts is quite relevant to the binding strength of BA on the catalysts (See [Table S4](#) and the
22 related discussion for more details in the [supporting information](#)).

23
24
25
26
27
28
29
30
31
32
33
34
35
36
37
38
39
40
41
42
43
44
45
46
47
48 It is noteworthy that excessive large adsorption energy could lead to relatively lower activity
49 according to the Sabatier principle.⁴¹ The activities and adsorption energies for RuPd/CN and
50 Ru/CN seem to be self-contradictory, due to the fact that RuPd/CN possesses relatively larger
51 adsorption energy, while maintains a better activity than Ru/CN. In fact, the paradox is induced
52
53
54
55
56
57
58
59
60

by the different amount of active sites in different catalysts, which can be verified through XPS analysis (Table 3). Compared with Ru/CN, the increased $\text{Ru}^0/\text{Ru}^{n+}$ ratio in RuPd/CN occurred after the formation of RuPd alloy, which may be conducive to the enhanced activity of RuPd/CN.

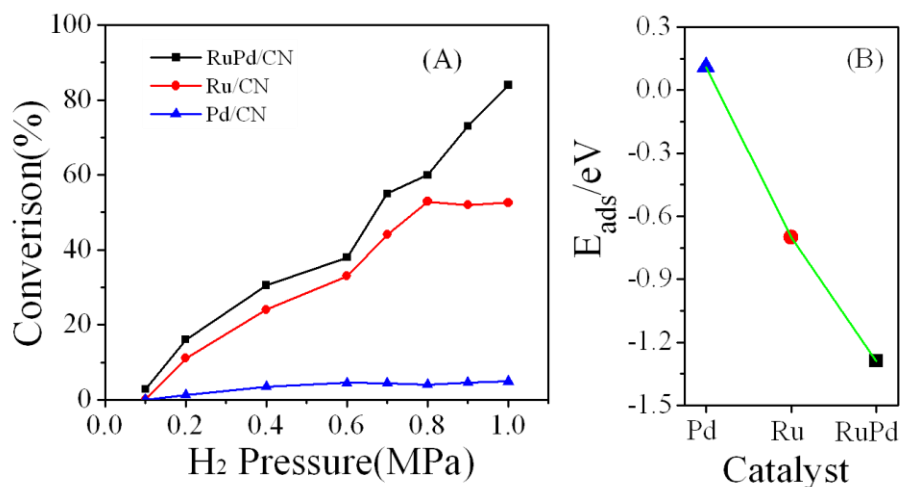
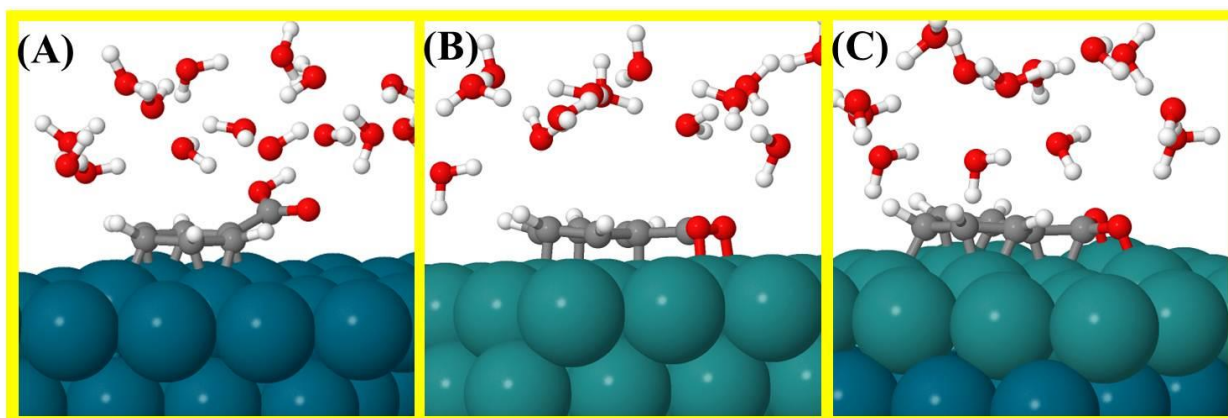


Figure 6. (A) Influence of hydrogen pressure on BA conversion with different catalysts. Reaction conditions: BA 1 mmol, catalyst 25 mg, solvent water 25 mL, 55 °C, 1 h. (B) The adsorption energies of BA on different catalysts derived from DFT calculations.



1
2
3 **Figure 7.** The optimized adsorption modes of BA in the water solvent on (A) Pd, (B) Ru and (C)
4 RuPd catalysts, respectively. Dark green: Pd, light green: Ru, grey: carbon, red: oxygen, and
5
6 white: hydrogen.
7
8

9
10
11
12 Anderson¹⁶ and Bai⁴² proposed that the polar carboxyl group of BA is repulsive to the catalyst
13 and faces upward to the polar solvent, such as water. However, the calculation results performed
14 here provides a distinguishing insight. When excluding the solvent, the optimized structures of
15 the chemisorption of BA on the three catalysts, reflect that the C=O of the carboxyl group
16 (COOH) binds on the catalyst surface indeed apart from Pd (see [Figure S2](#)). Considering the
17 conducting experimental conditions, the adsorption modes of BA on the catalysts were
18 recalculated by introducing the effects of solvation (see Figure 7). The adsorption mode of BA
19 on Pd mostly remains the same, while it is not the case for Ru and RuPd catalysts. The hydrogen
20 (H) atom in COOH dissolves into the solvent due to the ionization of water and the two oxygen
21 (O) atoms in reserve both bind to the surfaces of the catalysts. It can be concluded that the
22 configuration of COOH in chemisorbed BA in water solvent is determined by both the nature of
23 the catalysts and the effects of the solvation, through the comparison of the BA adsorption modes
24 among the three catalysts. To be exact, the adsorption mode of the C=O fragment is in all
25 probability affected only by the nature of the catalysts rather than the effects of the solvation
26 since its configuration changes little in both vacuum and water solvent on each catalyst.
27 However, the adsorption mode of the OH fragment is likely influenced by both factors since the
28 H atom of COOH in vacuum dissolves into water solvent on Ru and RuPd while it remains on Pd
29 in both cases. Unfortunately, it is hard to get the adsorption energy of BA in water solvent due to
30 the numerous relative configurations among the water molecules. Therefore the charge transfer is
31
32
33
34
35
36
37
38
39
40
41
42
43
44
45
46
47
48
49
50
51
52
53
54
55
56
57
58
59
60

1
2
3 utilized as the chemisorption strength descriptor here, rather than the adsorption energy. As can
4
5 be seen in [Table S4](#), the charge transfer of BA or the relevant acid ion changes only a little in
6
7 water solvent compared with that in vacuum. So it is rational to deduce that the trend of the
8
9 distinguishing adsorption energies of BA on different catalysts remains the same in water solvent.
10
11 This is why the adsorption energies of BA on the catalysts in vacuum are used to study the
12
13 platform.
14
15

16
17 The excellent selectivity for BA hydrogenation on the three catalysts is obviously interesting.
18
19 In other words, the reason why the COOH group does not undergo the hydrogenation process is
20
21 of great important. Figure 7 probably can explain in part. In water solvent, the H atom in COOH
22
23 of BA which chemisorbed on Ru and RuPd catalysts respectively dissolves into water
24
25 spontaneously, which means COOH of BA more likely tends to release a H atom rather than
26
27 receive one. Furthermore, we calculated the thermodynamics of COOH dissociation and
28
29 hydrogenation respectively, in vacuum for simplicity. The energy results are shown in Table 5.
30
31 For Pd, the positive COOH hydrogenation and dissociation energies which mean endothermic
32
33 reactions, imply that COOH tends to maintain itself since the surface H atoms from dissociated
34
35 H₂ molecules prefer to stay on the surface rather than bind to COOH and dissociation of COOH
36
37 is thermodynamically unfavourable under low temperatures. For Ru and RuPd, the positive
38
39 COOH hydrogenation and negative dissociation energies indicate that COOH
40
41 thermodynamically intends to dissociate the H atom resulting in two O atoms binding to the
42
43 catalyst surfaces. In conclusion, the hydrogenation of COOH is thermodynamically favorable in
44
45 none of the cases.
46
47
48
49
50
51
52
53
54
55
56
57
58
59
60

Table 5. The thermodynamics of hydrogenation and dissociation of COOH in BA. Negative value means exothermic reaction and positive value means the opposite. The relevant optimized structures studied for COOH hydrogenation and dissociation can be seen in [Figure S3](#).

Catalysts	Pd	Ru	RuPd
Hydrogenation	0.36	0.79	0.20
Dissociation	0.65	-0.53	-0.29

Gratifyingly, RuPd/CN also showed impressive activity in the hydrogenation of benzoic acid derivatives ([Table S6](#)). In a final set of experiments, the reusability of RuPd/CN contrast with commercial Pd/AC (Pd loading is 5 wt. %) was investigated ([Figure 8](#)). Results revealed that after easy separation and pretreatment, RuPd/CN still could achieve a high conversion of 85% after four batches, demonstrating its good deactivation resistance and recyclability. While for commercial Pd/AC, there was a considerable decrease in catalytic activity during these recycling tests. Furthermore, no traces of leached Ru or Pd species were detected in the reaction filtrate of RuPd/CN as catalyst. These results demonstrated that the highly active RuPd/CN was more stable than commercial Pd/AC under the investigated conditions. Its excellent catalytic performance and good recyclability will make the RuPd/CN catalyst attractive for both fundamental research and practical applications.

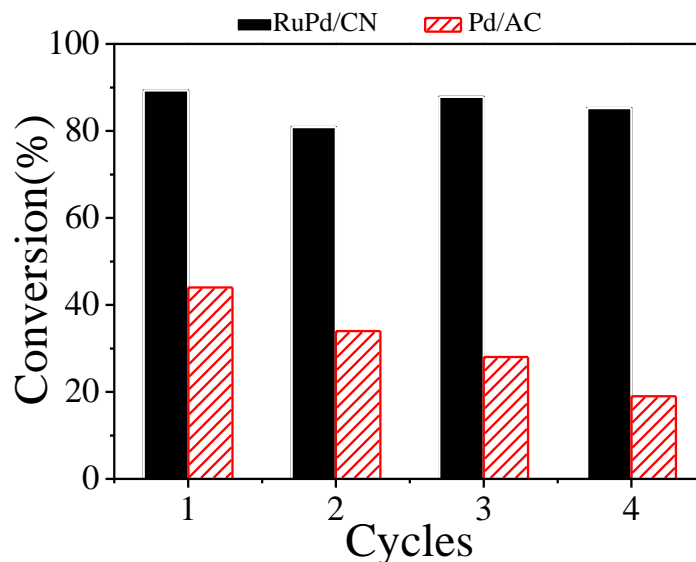


Figure 8. Comparison of the reusability of the RuPd/CN and commercial Pd/AC in the BA hydrogenation under the same reaction conditions. Reaction conditions: BA 0.75 mmol, catalyst 50 mg, solvent water 25 mL, 55 °C, 0.4 MPa H₂ pressure, 1 h.

3. CONCLUSIONS

Alloyed RuPd/CN catalyst was prepared via a simple ultrasound-assisted co-reduction technique, exhibiting a remarkably superior activity and excellent stability over their monometallic counterparts for the hydrogenation of BA under mild conditions. The excellent catalytic performance was mainly attributed to the increased Ru⁰/Ruⁿ⁺ ratio induced by RuPd formation confirmed by various characterizations. The platform on the activity to the H₂ pressure present different phenomenon on different catalysts was further explained by calculating the adsorption energy of BA on the catalysts from a first-principle view. And the unique phenomenon was due to the relatively strong adsorption energies of BA on the RuPd/CN. The factors influencing the adsorption modes of BA, especially the configuration of the carboxyl group are investigated preliminarily in first principle, giving a distinct view from the former

1
2
3 work. The reason why the carboxyl group in BA does not undergo hydrogenation, which results
4 in the superior selectivity (>99%), is also revealed by the comparisons of the thermodynamics of
5 hydrogenation and dissociation of the carboxyl group. In addition, the strategy reported here
6 provides a means for seeking more economical metal elements alloying with noble metal to
7 prepare bimetallic catalysts, which are applicable for various hydrogenation reactions, with
8 superior catalytic performance.
9
10
11
12
13
14
15
16
17
18
19

20 **4. EXPERIMENTAL SECTION**

21 **4.1. Catalyst preparation**

22
23
24 The N-doped carbon (CN) was synthesized as described previously.²⁵ Bimetallic MPd/CN
25 (M=Ru, Cu, Fe, Ni and In) and RuM/CN (M=Cu, Fe, Ni and In) catalysts were prepared by
26 ultrasound-assisted co-reduction method. Taking the typical synthesis of RuPd/CN as an
27 example, appropriate amounts of CN was dispersed in deionized water in a beaker under
28 ultrasound, and then desired amount RuCl₃ aqueous solution (0.01 g/mL) and Na₂PdCl₄ aqueous
29 solution (0.01 g/mL) were added into the beaker under treatment in ultrasound for 10 minutes.
30 Then 10 mL freshly prepared NaBH₄ aqueous solution (2 mg/mL) was added to the suspension
31 under ultrasound treatment for another 30 minutes. The solid were separated from the solution by
32 filtration and washed with water thoroughly. The obtained catalysts were dried at 70 °C overnight,
33 and then it was treated with a simple grinding and denoted as RuPd/CN. Pd/CN and Ru/CN were
34 prepared using the same methodology for comparison.
35
36
37
38
39
40
41
42
43
44
45
46
47
48
49
50

51 **4.2. Catalyst characterization**

52
53 The BET specific surface areas were measured on a surface area and porosity analyzer
54 (Micromeritics, ASAP 2020 HD88). Actual content of Ru and Pd in the prepared catalysts were
55
56
57
58
59
60

1
2
3 measured by inductively coupled plasma-atomic emission spectroscopy (ICP-AES) on a Plasma-
4 Spec-II spectrometer. The dispersion of Pd was calculated on the basis of CO chemisorption at
5 room temperature, using a CHEMBET-3000 apparatus (Quantachrome Co.). High-resolution
6 transmission electron microscopy (HRTEM) was carried out on an FEI Tecnai G2 F20 S-TWIN
7 microscope. High-resolution scanning transmission electron microscopy (HRSTEM) high-angle
8 annular dark-field (HAADF)-STEM and EDX analyses were recorded on a Titan G280-200 w/
9 ChemiSTEM instrument. X-ray power diffraction analysis (XRD) was performed using Ultima
10 TV X-ray diffractometer with Cu K α radiation (1.54 Å). The X-ray photoelectron spectra (XPS)
11 were obtained by an ESCALAB MARK II spherical analyzer using an aluminum-magnesium
12 binode (Al 1486.6 eV, Mg 1253.6 eV) X-ray source. Hydrogen temperature-programmed
13 reduction (H₂-TPR) was conducted in FINESORB-3010 apparatus equipped with a thermal
14 conductivity detector (TCD). Before a TPR run, catalysts were pretreated in Ar at 473 K for 2
15 hours. TPR was performed in a flow of 10% H₂/Ar mixture gas at a flow rate of 10 sccm with a
16 temperature ramp of 10 °C /min.
17
18
19
20
21
22
23
24
25
26
27
28
29
30
31
32
33
34
35

36 **4.3. Hydrogenation of BA**

37
38 In a typical process, 0.5 mmol BA and 50 mg RuPd/CN were put into a three-neck flask, and
39 25 mL deionized water was employed as a green solvent. The reaction was carried out at a
40 temperature of 85 °C with magnetic stirring at a speed of 1000 rpm. Before reaction, a balloon
41 filled with hydrogen was connected to the flask to replace the air. After the reaction, the contents
42 of products and substrate were determined by GC-FID and the products were identified by GC-
43 MS.
44
45
46
47
48
49
50
51

52 **4.4. Computational setup**

1
2
3 The calculations reported here are performed by using periodic, spin-polarized DFT as
4 implemented in Vienna ab initio program package (VASP).^{43,44} The electron-ion interactions are
5 described by the projector augmented wave (PAW) method proposed by Blöchl⁴⁵ and
6 implemented by Kresse⁴⁶. RPBE functional⁴⁷ is used as exchange-correlation functional
7 approximation and a plane wave basis set with an energy cutoff of 400 eV is used. Only gamma
8 point is used for the Brillouin zone sampling, during the structure optimization, while a kpoint of
9 3*3*1 is used for bader charge analysis⁴⁸. A p (5×5) supercell containing a four-layer slab with
10 100 atoms was modeled. The periodic condition is employed along the x and y direction. The
11 vacuum space along the z direction was set to be 13 Å. For RuPd catalyst, Pd was alloyed to the
12 sub-layer of Ru catalyst ([Figure S1](#)). The upper two layer atoms in the cell are allowed to relax
13 during the structure optimization and the bottom two layer atoms are fixed. When solvent, i.e.
14 water is considered, two water layers with 17 water molecules are introduced to simulate a
15 similar density of liquid water phase. The relaxation is stopped when the force residue on the
16 atom is smaller than 0.02 eV/Å. The adsorption energy for BA chemisorption is defined as:

$$E_{\text{ads}} = E_{\text{tot}} - E_{\text{slab}} - E_{\text{BA}}$$

17
18
19
20
21
22
23
24
25
26
27
28
29
30
31
32
33
34
35
36
37
38
39
40
41
42
43 Where E_{tot} is the total energy after BA adsorption the on catalysts; E_{slab} is the energy of the
44 clean catalyst alone; E_{BA} is the energy of BA in the gas phase.
45
46
47
48
49
50
51
52

53 ASSOCIATED CONTENT

56 Supporting Information.

1
2
3 Experimental details, ICP-AES results, curve fitting of N₂ adsorption-desorption isotherms,
4
5 HRTEM images of Ru/CN and Pd/CN catalysts, the effect of time and solvents on the catalysts
6
7 activity, the hydrogenation of benzoic acid derivatives in Supporting Information. This material is
8
9 available free of charge via the Internet at <http://pubs.acs.org>.
10
11
12
13
14
15
16
17

18 AUTHOR INFORMATION

20 Corresponding Author

21
22
23 * E-mail: chemwy@zju.edu.cn. Fax: +86-571-87951895.
24
25

26 Notes

27
28
29 The authors declare no competing financial interest.
30
31
32

33 ACKNOWLEDGMENT

34
35
36 Financial support from the National Natural Science Foundation of China (21376208), the
37
38 Zhejiang Provincial Natural Science Foundation for Distinguished Young Scholars of China
39
40 (LR13B030001), the Specialized Research Fund for the Doctoral Program of Higher Education
41
42 (J20130060), the Fundamental Research Funds for the Central Universities, the Program for
43
44 Zhejiang Leading Team of S&T Innovation, the Partner Group Program of the Zhejiang
45
46 University and the Max-Planck Society are greatly appreciated.
47
48
49
50
51
52

53 REFERENCES

54
55
56 (1) Moore, B. S.; Cho, H.; Casati, R.; Kennedy, E.; Reynolds, K. A.; Mocek, U.; Beale, J. M.;
57
58 Floss, H. G., *J. Am. Chem. Soc.* **1993**, *115*, 5254-5266.
59
60

- 1
2
3
4 (2) Temkin, M.; Konyukhov, V. Y.; Kul'kova, N., *JOURNAL OF THE RESEARCH*
5 *INSTITUTE FOR CATALYSIS HOKKAIDO UNIVERSITY* **1981**, *28*, 363-370.
- 6 (3) Anderson, J.; McKenna, F.-M.; Linares-Solano, A.; Wells, R. K., *Catal. Lett.* **2007**, *119*,
7 16-20.
- 8 (4) Gaude, D.; Le Goaller, R.; Luche, J.-L.; Pierre, J.-L., *Tetrahedron Lett.* **1984**, *25*, 5897-
9 5898.
- 10 (5) Wang, H.; Zhao, F., *Int. J. Mol. Sci.* **2007**, *8*, 628-634.
- 11 (6) Claus, P.; Berndt, H.; Mohr, C.; Radnik, J.; Shin, E.-J.; Keane, M. A., *J. Catal.* **2000**, *192*,
12 88-97.
- 13 (7) Cervantes, G. G.; Aires, F. C. S.; Bertolini, J., *J. Catal.* **2003**, *214*, 26-32.
- 14 (8) Cabiac, A.; Delahay, G.; Durand, R.; Trens, P.; Coq, B.; Plée, D., *Carbon* **2007**, *45*, 3-10.
- 15 (9) Panpranot, J.; Kontapakdee, K.; Praserttham, P., *J. Phys. Chem. B*, **2006**, *110*, 8019-8024.
- 16 (10) Panpranot, J.; Pattamakomsan, K.; Goodwin Jr, J. G.; Praserttham, P., *Catal. Commun.*
17 **2004**, *5*, 583-590.
- 18 (11) Wang, Y.; Yao, J.; Li, H.; Su, D.; Antonietti, M., *J. Am. Chem. Soc.* **2011**, *133*, 2362-2365.
- 19 (12) Ueno, T.; Suzuki, M.; Goto, T.; Matsumoto, T.; Nagayama, K.; Watanabe, Y., *Angew.*
20 *Chem.* **2004**, *116*, 2581-2584.
- 21 (13) Liu, H.; Jiang, T.; Han, B.; Liang, S.; Zhou, Y., *Science* **2009**, *326*, 1250-1252.
- 22 (14) Zhao, C.; Kou, Y.; Lemonidou, A. A.; Li, X.; Lercher, J. A., *Angew. Chem.* **2009**, *121*,
23 4047-4050.
- 24 (15) Xu, X.; Li, Y.; Gong, Y.; Zhang, P.; Li, H.; Wang, Y., *J. Am. Chem. Soc.* **2012**, *134*,
25 16987-16990.
- 26 (16) Anderson, J. A.; Athawale, A.; Imrie, F. E.; McKenna, F. M.; McCue, A.; Molyneux, D.;
27 Power, K.; Shand, M.; Wells, R. P. K., *J. Catal.* **2010**, *270*, 9-15.
- 28 (17) Amadou, J.; Chizari, K.; Houllé, M.; Janowska, I.; Ersen, O.; Bégin, D.; Pham-Huu, C.,
29 *Catal. Today* **2008**, *138*, 62-68.
- 30 (18) Elías, A. L.; Botello-Méndez, A. s. R.; Meneses-Rodríguez, D.; Jehová González, V.;
31 Ramírez-González, D.; Ci, L.; Muñoz-Sandoval, E.; Ajayan, P. M.; Terrones, H.; Terrones, M.,
32 *Nano Lett.* **2009**, *10*, 366-372.
- 33 (19) Zhang, P.; Yuan, J.; Fellingner, T.-P.; Antonietti, M.; Li, H.; Wang, Y., *Angew. Chem., Int.*
34 *Ed.* **2013**, *52*, 6028-6032.
- 35 (20) Liu, R.; Mahurin, S. M.; Li, C.; Unocic, R. R.; Idrobo, J. C.; Gao, H.; Pennycook, S. J.;
36 Dai, S., *Angew. Chem., Int. Ed.* **2011**, *50*, 6799-6802.
- 37 (21) Yang, S.; Feng, X.; Wang, X.; Müllen, K., *Angew. Chem., Int. Ed.* **2011**, *50*, 5339-5343.
- 38 (22) Yang, W.; Fellingner, T.-P.; Antonietti, M., *J. Am. Chem. Soc.* **2010**, *133*, 206-209.
- 39 (23) Fulvio, P. F.; Lee, J. S.; Mayes, R. T.; Wang, X.; Mahurin, S. M.; Dai, S., *Phys. Chem.*
40 *Chem. Phys.* **2011**, *13*, 13486-13491.
- 41 (24) Lee, J. S.; Wang, X.; Luo, H.; Baker, G. A.; Dai, S., *J. Am. Chem. Soc.* **2009**, *131*, 4596-
42 4597.
- 43 (25) Xu, X.; Tang, M.; Li, M.; Li, H.; Wang, Y., *ACS Catal.* **2014**, *4*, 3132-3135.
- 44 (26) Yang, X.; Chen, D.; Liao, S.; Song, H.; Li, Y.; Fu, Z.; Su, Y., *J. Catal.* **2012**, *291*, 36-43.
- 45
46
47
48
49
50
51
52
53
54
55
56
57
58
59
60

- 1
2
3
4 (27) Henning, A. M.; Watt, J.; Miedziak, P. J.; Cheong, S.; Santonastaso, M.; Song, M.;
5 Takeda, Y.; Kirkland, A. I.; Taylor, S. H.; Tilley, R. D., *Angew. Chem., Int. Ed.* **2013**, *52*, 1477-
6 1480.
- 7 (28) Hirasawa, S.; Watanabe, H.; Kizuka, T.; Nakagawa, Y.; Tomishige, K., *J. Catal.* **2013**,
8 *300*, 205-216.
- 9 (29) Hermannsdörfer, J.; Friedrich, M.; Miyajima, N.; Albuquerque, R. Q.; Kümmel, S.;
10 Kempe, R., *Angew. Chem., Int. Ed.* **2012**, *51*, 11473-11477.
- 11 (30) Vicente, A.; Lafaye, G.; Especel, C.; Marécot, P.; Williams, C. T., *J. Catal.* **2011**, *283*,
12 133-142.
- 13 (31) Sun, J.; Karim, A. M.; Zhang, H.; Kovarik, L.; Li, X. S.; Hensley, A. J.; McEwen, J.-S.;
14 Wang, Y., *J. Catal.* **2013**, *306*, 47-57.
- 15 (32) Lee, J.; Kim, Y. T.; Huber, G. W., *Green Chem.* **2014**, *16*, 708-718.
- 16 (33) Jin, X.; Dang, L.; Lohrman, J.; Subramaniam, B.; Ren, S.; Chaudhari, R. V., *ACS Nano*
17 **2013**, *7*, 1309-1316.
- 18 (34) Son, S. U.; Jang, Y.; Park, J.; Na, H. B.; Park, H. M.; Yun, H. J.; Lee, J.; Hyeon, T., *J. Am.*
19 *Chem. Soc.* **2004**, *126*, 5026-5027.
- 20 (35) Wang, C.; Li, B.; Lin, H.; Yuan, Y., *J. Power Sources* **2012**, *202*, 200-208.
- 21 (36) Luo, G.; Yan, S.; Qiao, M.; Zhuang, J.; Fan, K., *Appl. Catal. A: Gen.* **2004**, *275*, 95-102.
- 22 (37) Kusada, K.; Kobayashi, H.; Ikeda, R.; Kubota, Y.; Takata, M.; Toh, S.; Yamamoto, T.;
23 Matsumura, S.; Sumi, N.; Sato, K.; Nagaoka, K.; Kitagawa, H., *J. Am. Chem. Soc.* **2014**, *136*,
24 1864-1871.
- 25 (38) Fang, M.; Machalaba, N.; Sanchez-Delgado, R. A., *Dalton Transactions* **2011**, *40*, 10621-
26 10632.
- 27 (39) Sá, J.; Arteaga, G. D.; Daley, R. A.; Bernardi, J.; Anderson, J. A., *The J. Phys. Chem. B*
28 **2006**, *110*, 17090-17095.
- 29 (40) da-Silva, J. W.; Cobo, A. J. G., *Appl. Catal. A: Gen.* **2003**, *252*, 9-16.
- 30 (41) Knözinger, H.; Kochloefl, K., Heterogeneous Catalysis and Solid Catalysts. In *Ullmann's*
31 *Encyclopedia of Industrial Chemistry*, Wiley-VCH Verlag GmbH & Co. KGaA: 2000.
- 32 (42) Bai, G.; Wen, X.; Zhao, Z.; Li, F.; Dong, H.; Qiu, M., *Ind. Eng. Chem. Res.* **2013**, *52*,
33 2266-2272.
- 34 (43) Kresse, G.; Furthmüller, J., *Comp. Mater. Sci.* **1996**, *6*, 15-50.
- 35 (44) Kresse, G.; Furthmüller, J., *Phys. Rev. B* **1996**, *54*, 11169.
- 36 (45) Blöchl, P. E., *Phys. Rev. B* **1994**, *50*, 17953.
- 37 (46) Kresse, G.; Joubert, D., *Phys. Rev. B* **1999**, *59*, 1758.
- 38 (47) Hammer, B.; Hansen, L. B.; Nørskov, J. K., *Phys. Rev. B* **1999**, *59*, 7413.
- 39 (48) Bader, R. F. W., *Atoms in Molecules*. In *Encyclopedia of Computational Chemistry*: John
40 Wiley & Sons, Ltd: 2002.
- 41
42
43
44
45
46
47
48
49
50
51
52
53
54
55
56
57
58
59
60

